International Journal of Heat and Mass Transfer 209 (2023) 124144

Contents lists available at ScienceDirect

International Journal of Heat and Mass Transfer

journal homepage: www.elsevier.com/locate/hmt

Entropy generation analysis of a three-dimensional coal-fired furnace: A realistic study

Zhongnong Zhang[a], Nimeti Doner[a,b,*], Chun Lou[a,*], Chong Zhang[a]

[a] State Key Laboratory of Coal Combustion, School of Energy and Power Engineering, Huazhong University of Science and Technology, Wuhan, 430074 Hubei, China

[b] Mechanical Engineering Department, Engineering Faculty, Gazi University, 06570 Ankara, Turkey

ARTICLE INFO

Article history:
Received 15 December 2022
Revised 22 March 2023
Accepted 23 March 2023
Available online 29 March 2023

Keywords:
Entropy generation
Radiative heat transfer
Coal-fired furnace
Gas
Particle

ABSTRACT

An analysis of the entropy generation by radiative heat transfer in a three-dimensional virtual coal-fired furnace is performed. The gases, including CO_2 and H_2O, and particles, including soot, unburnt char and ash, are considered as a participating medium. The radiative transfer equation for a non-grey medium was solved by the discrete ordinate method, in which the radiative properties of the gases, soot, unburnt char and ash were obtained by using the statistical narrow-band correlated-k model, Rayleigh's theory, and Mie theory, respectively. The distributions of the local volumetric rate of entropy generation and the local rate of entropy generation at the wall are calculated. The contributions of various media in coal-burning furnaces to the radiative entropy generation rate (REGR) are evaluated, and the effects of several important factors, such as the oxidizer atmosphere, burnout rate, and the volume fraction of soot, unburnt char and ash on the REGR and dimensionless entropy generation were also investigated. The numerical results show that the irreversibility of the particle radiation contributes more than 80% of the volumetric radiative entropy generation. The concentration of particles also has an important effect on REGR, which decreases by 41% when the concentration of unburnt char and ash increases from 10 ppm to 50 ppm and decreases by 70% when the concentration of soot increases from 1 ppm to 6 ppm in a real-size furnace such as an optically thick furnace.

© 2023 Elsevier Ltd. All rights reserved.

1. Introduction

The main purposes of energy utilization systems are to accomplish the conversion of energy and to obtain available work. However, the thermodynamic irreversibility of the combustion process leads to a certain loss of available work, and is characterized by the entropy generation parameter [1]. Sciacovelli et al. [2] explained in detail the effects of contribution of entropy generation to system design in their review study. Two methods, namely black box modelling and entropy generation analysis, can be used for the design of systems with heat and mass transfer. They mentioned that there is a strong and explicit relation between entropy generation and the physical properties of the system. Based on the analysis of various thermal systems, the authors concluded that the causes of inefficiency can be directly identified by entropy generation analysis, allowing designers to design more efficient systems. In high-temperature systems, thermal radiation is the dominant mode of heat transfer and is also a critical source of thermodynamic irreversibility [3,4]. Hence, it is of great interest to investigate the radiative entropy generation in high-temperature systems.

The study of radiation entropy has been discussed for a long time [5]. Radiation beams carry not only energy, but also entropy [6]. The entropy flux and entropy generation of black-body and grey-body radiation as well as the radiative heat transfer on a solid surface have been investigated. Wright et al. [7] investigated the calculation of spectral radiative behavior for systems using some issues such as inherent irreversibility, definition of the environment, the effect of inherent emission and the effect of concentrating the source radiation. Zhang and Basu [8] applied the entropy generation method to radiative transfer between surfaces in a solar system and showed that the method gives good results. The radiative heat transfer in a participating medium due to the irreversibility of emission, absorption and scattering was analysed using numerical solution of the radiative entropy transfer equation by Caldas and Semião [9]. The authors found that entropy production was lower in the less participating part of the studied domain, while entropy production was higher in the part with

* Corresponding author.
E-mail addresses: nimetidoner@gazi.edu.tr (N. Doner), Lou_chun@sina.com (C. Lou).

https://doi.org/10.1016/j.ijheatmasstransfer.2023.124144
0017-9310/© 2023 Elsevier Ltd. All rights reserved.

a strong temperature gradient and absorption-scattering properties. In the second work of the authors, the entropy generation method was applied to the turbulence-radiation interaction in a 2D channel [10]. Based on the results of a theoretical analysis, Liu and Chu [11,12] reported a verification of the numerical solution of the radiative entropy transfer equation using two examples (optical thicknesses are 1 and 3; ε=0.5, constant T_{wall}=1000 K) with semitransparent media in a two-dimensional radiative heat transfer system. They found that for both examples, the dimensionless spectral entropy generation is 0.7, which depends only on the temperature of the wall and the medium and not on other parameters, and that the method should be spectrally evaluated. Zhang et al. [13,14] analysed radiative heat transfer in thermal equilibrium and non-equilibrium, in the grey and non-grey participating medium. The effects of some parameters, including emissivity, optical thickness, and scattering albedo, on radiative entropy generation were analysed.

In almost all of these studies, generally the participating medium was assumed to just contain the gases, and only Bahrami et al. [15] and Zhang et al. [16] took into account the effect of soot particles in a one-dimensional radiative system. In [15], five different situations were tested in the form of homogeneous and non-homogeneous cases with only one participant gas and a homogeneous case including a homogeneous mixture of gas and soot. They showed that low temperature walls are a source of radiative entropy generation. Another important result was that the soot particles increased the radiative entropy generation. In practice, besides the gases and soot particle produced during combustion, the unburned char and ash particle in the coal-fired furnace also has an important impact on the radiative heat transfer [3,17–19]. These further affect the irreversibility of the radiation process, and should be considered in the thermodynamic analysis.

The calculation of the radiative entropy generation rate (REGR) relies on accurate numerical simulation results for the radiative heat transfer. The radiative heat transfer in an industrial furnace is extremely complicated. The radiative properties of the gases produced during combustion have strong non-grey characteristics, and the cost of the computational resources is prohibitive when the traditional numerical method line-by-line (LBL) model is applied, especially for solving for a high-dimensional combustion system [3,20]. Hence, a series of simplified models of gas radiative properties have been developed to reduce the calculation time, and have been also used in studies of the entropy generation of radiative heat transfer in gases [21,22], such as the statistical narrow-band correlated-k model (SNBCK) and the full-spectrum correlated-k (FSCK) model. The reported experimental data on the complex refractive index of fly ash show significant fluctuations in the wavelength range of 1–5 μm, further leading to the strong non-grey characteristics of ash in this band [23–26]. The radiative properties of unburnt char and ash can be obtained, and several models of the radiative properties of grey and non-grey particles have been developed based on particle size and radiation spectra [27–29]. Additionally, similarly to unburnt char and ash particle, soot particles also emit continuous thermal radiation across the entire infrared spectrum [30]. In terms of numerical calculations, the spectral absorption coefficient of soot is always considered to be approximately linear with respect to the wavenumber and volume according to the Rayleigh theory [3,31,32].

The aims of this paper are to investigate the radiative entropy generation in a three-dimensional (3-D) coal-fired furnace filled with non-grey gases and particles, and to analyse the influence of all these components on this generation. In this paper, a mixed medium consisting of H_2O, CO_2, soot, and unburned char and ash particles is considered, and the entropy generation due to the radiative properties of the gases and particles are calculated. Furthermore, the effects of the oxidizer atmosphere, the burnout rate, and concentration of the particles on the irreversibility of the radiative heat transfer process are analysed. Finally, some key conclusions are presented.

2. Numerical models and formulation

2.1. Radiative model of gases

The SNBCK model was used to solve for the radiative properties of non-grey gases in the radiative heat transfer equation. In this model, the total spectrum is divided into multiple narrow bands, in which the spectral radiative intensity of a black body is considered to be constant. In each band, the actual spectral radiative properties of gases can be expressed by the f distribution and the g distribution, where $g(k) = \int_0^k f(k')\mathrm{d}k'$. An analytical expression for these distributions can be given as:

$$g(k) = \frac{1}{2}\left[1 - \mathrm{erf}\left(\frac{a}{\sqrt{k}} - b\sqrt{k}\right)\right] + \frac{1}{2}\left[1 - \mathrm{erf}\left(\frac{a}{\sqrt{k}} - b\sqrt{k}\right)\right]e^{\pi B} \tag{1}$$

where $a = (\pi Y p \bar{k}_\nu \bar{\gamma}_\nu / \bar{\delta}_\nu)^{0.5}$, $b = (\pi \bar{\gamma}_\nu / (Y p \bar{k}_\nu \bar{\delta}_\nu))^{0.5}$, Y is the mole fraction of the gas, p is the gas pressure, and $\bar{\gamma}_\nu$, $\bar{k}_\nu$, and $\bar{\delta}_\nu$ are the parameters of the gas, as presented in a previous work [22].

Based on the assumptions of the SNBCK model, the radiative intensity corresponding to the value of the distribution function g in the narrowband ($\Delta\eta$) $I_{g,\Delta\eta}$ can be obtained by solving the radiative transfer equation (RTE). Furthermore, the average spectral radiative intensity can be obtained by integrating $I_{g,\Delta\eta}$ along the values of the g distribution function. Since the g distribution function increases monotonically, the calculation of the average radiative intensity can be effectively simplified by using a Gauss-Lobatto quadrature scheme.

2.2. Radiative model of unburnt char and ash

Mie theory is used for the calculation of the spectral radiative property of unburnt char and ash particle. Based on independent scattering conditions, the absorption and scattering coefficients of unburnt char and ash particle ($\kappa_{\eta,\mathrm{ac}}$ and $\sigma_{\eta,ac}$) are calculated as follows:

$$\kappa_{\eta,ac} = 1.5\sum_{i=1}^{n} Q_{abs,\eta}(D_p)\frac{f_{v,ac}}{D_p} \tag{2}$$

$$\sigma_{\eta,ac} = 1.5\sum_{i=1}^{n} Q_{sca,\eta}(D_p)\frac{f_{v,ac}}{D_p} \tag{3}$$

where $Q_{abs,\eta}$ and $Q_{sca,\eta}$ are the absorption efficiency and scattering efficiency, which can be determined by Mie theory with known the size parameter and the complex refractive index [24,25], D_p and $f_{v,ac}$ are the diameter and volume fraction of unburnt char and ash particle, and can be obtained through a simplified calculation for the coal-fired furnace [27].

2.3. Radiative model of soot

Soot is generated due to incomplete combustion of fuel and it emits continuous thermal radiation in the entire visible and infrared spectrum band. In this paper, soot particle in the furnace is considered as spherical and well dispersed. Meanwhile, since the soot particle is very small, the scattering process of soot is negligible. The absorption coefficient of soot $\kappa_{\eta,soot}$ is linearly related to the wavenumber and soot volume fraction according to Rayleigh's theory, and the detailed relationship is given as:

$$\kappa_{\eta,soot} = C f_{v,soot}\eta \tag{4}$$

where $f_{v,soot}$ is the volume fraction of the soot particle, η is the wavenumber and C is a constant for which values between 3.5 and 7.5 can be obtained for coal combustion [31,32].

2.4. Solution of radiative transfer equation

To calculate the radiative intensities in a three-dimensional coal-fired furnace including an absorbing, emitting and isotropic scattering [$\Phi(s, s')$=1] gas-particle media, the RTE is written as follow [3]. In addition, the effects of radiative heat transfer by out-scattering and in-scattering are expressed in the RTE by the fourth term and the last term on the right side of the equation:

$$\frac{dI_\eta(\mathbf{r},\mathbf{s})}{ds} = \kappa_{\eta,g}(\mathbf{r})I_b(T_g(\mathbf{r})) + \kappa_{\eta,p}(\mathbf{r})I_b(T_p(\mathbf{r})) - \left[\kappa_{\eta,g}(\mathbf{r}) + \kappa_{\eta,p}(\mathbf{r})\right]I_\eta(\mathbf{r},\mathbf{s}) - \sigma_{\eta,ac}(\mathbf{r})I_\eta(\mathbf{r},\mathbf{s}) + \frac{\sigma_{\eta,ac}(\mathbf{r})}{4\pi}\int_{4\pi}\Phi(\mathbf{s},\mathbf{s}')I_\eta(\mathbf{r},\mathbf{s}')d\mathbf{s}' \quad (5)$$

where I_η is the spectral radiative intensity, T_g and T_p are the temperatures of the gas and particles, respectively, $\kappa_{\eta,g}$ and $\kappa_{\eta,p}$ are the spectral absorption coefficients of the gas and particles, respectively, and can be given as:

$$\kappa_{\eta,g} = \kappa_{\eta,CO_2} + \kappa_{\eta,H_2O} \quad (6)$$

$$\kappa_{\eta,p} = \kappa_{\eta,soot} + \kappa_{\eta,ac} \quad (7)$$

where κ_{η,CO_2}, κ_{η,H_2O} are the spectral absorption coefficients of CO_2, H_2O, respectively.

The combustion process in the furnace is considered to be in a state of thermal equilibrium. Therefore, the temperatures of the gas and particles are considered to be the same. Based on the SNBCK model of gas, the RTE in a narrow-band ($\Delta\eta$) can be rewritten as:

$$\frac{dI_{ij,\Delta\eta}(\mathbf{r},\mathbf{s})}{ds} = \left[k_{g_i,\Delta\eta,CO_2}(\mathbf{r}) + k_{g_j,\Delta\eta,H_2O}(\mathbf{r}) + \kappa_{\eta,p}(\mathbf{r})\right]I_b(\mathbf{r}) - \left[k_{g_i,\Delta\eta,CO_2}(\mathbf{r}) + k_{g_j,\Delta\eta,H_2O}(\mathbf{r}) + \kappa_{\eta,p}(\mathbf{r}) + \sigma_{\eta,ac}(\mathbf{r})\right]I_{g_i,\Delta\eta}(\mathbf{r},\mathbf{s}) + \frac{\sigma_{\eta,ac}(\mathbf{r})}{4\pi}\int_{4\pi}\Phi(\mathbf{s},\mathbf{s}')I_{g_i,\Delta\eta}(\mathbf{r},\mathbf{s}')d\mathbf{s}' \quad (8)$$

where $I_{g,\Delta\eta}$ is the corresponding radiative intensity under the distribution function value g in the narrow-band ($\Delta\eta$). I_b is the spectral radiative intensity of the black body and the subscript η is the central wavenumber in the narrow band $\Delta\eta$. Furthermore, the average radiative intensity in the narrow band ($\Delta\eta$) is given as:

$$\bar{I}_{\Delta\eta} = \sum_{i=1}^{N_q}\sum_{i=1}^{N_q}\omega_i\omega_j I_{ij,\Delta\eta} \quad (9)$$

where N_q is the number of quadrature points in the SNBCK model, and the seven-point Gauss-Lobatto quadrature scheme was used.

Additionally, the local radiative heat flux density q and total heat flux Q on the wall can be calculated as follows:

$$q(\mathbf{r}_W) = \sum_{\text{bands}}\int_{4\pi}\bar{I}_{\Delta\eta}(\mathbf{r}_W)(\mathbf{n}_W\cdot\mathbf{s})d\Omega\Delta\eta \quad (10)$$

$$Q = \int_W q(\mathbf{r}_W)dA \quad (11)$$

2.5. Formulation of radiative entropy generation

There are three sources of radiative entropy generation in high-temperature furnaces: the irreversibility of the absorption and emission processes in the medium, the irreversibility of the scattering process in the medium, and the irreversibility of the absorption, emission, and reflection processes at the wall. The entropy generation rates due to the irreversibility of the absorption and emission processes of gases and particles can be expressed as [33]:

$$S'''_{ae,CO_2}(\mathbf{r}) = -\sum_{\text{bands}}\int_\Omega\sum_{i=1}^{N_q}\sum_{j=1}^{N_q}\omega_i\omega_j k_{g_i,\Delta\eta,CO_2}\left[I_{b,\eta}(\mathbf{r}) - I_{\Delta\eta,ij}(\mathbf{r},\mathbf{s})\right]\left[\frac{1}{T(\mathbf{r})} - \frac{1}{T_{\eta,ij}(\mathbf{r},\mathbf{s})}\right]d\Omega\Delta\eta,$$

$$S'''_{ae,H_2O}(\mathbf{r}) = -\sum_{\text{bands}}\int_\Omega\sum_{i=1}^{N_q}\sum_{j=1}^{N_q}\omega_i\omega_j k_{g_j,\Delta\eta,H_2O}\left[I_{b,\eta}(\mathbf{r}) - I_{\Delta\eta,ij}(\mathbf{r},\mathbf{s})\right]\left[\frac{1}{T(\mathbf{r})} - \frac{1}{T_{\eta,ij}(\mathbf{r},\mathbf{s})}\right]d\Omega\Delta\eta,$$

$$S'''_{ae,soot}(\mathbf{r}) = -\sum_{\text{bands}}\int_\Omega\sum_{i=1}^{N_q}\sum_{j=1}^{N_q}\omega_i\omega_j\kappa_{\eta,\text{soot}}\left[I_{b,\eta}(\mathbf{r}) - I_{\Delta\eta,ij}(\mathbf{r},\mathbf{s})\right]\left[\frac{1}{T(\mathbf{r})} - \frac{1}{T_{\eta,ij}(\mathbf{r},\mathbf{s})}\right]d\Omega\Delta\eta,$$

$$S'''_{ae,ac}(\mathbf{r}) = -\sum_{\text{bands}}\int_\Omega\sum_{i=1}^{N_q}\sum_{j=1}^{N_q}\omega_i\omega_j\kappa_{\eta,\text{ac}}\left[I_{b,\eta}(\mathbf{r}) - I_{\Delta\eta,ij}(\mathbf{r},\mathbf{s})\right]\left[\frac{1}{T(\mathbf{r})} - \frac{1}{T_{\eta,ij}(\mathbf{r},\mathbf{s})}\right]d\Omega\Delta\eta, \quad (12)$$

where T_η is the spectral radiative temperature. S'''_{ae,CO_2}, S'''_{ae,H_2O}, $S'''_{ae,soot}(r)$, and $S'''_{ae,ac}$ represent the local radiative entropy generation due to the absorption and emission processes of the CO_2, H_2O, the soot particle, unburnt char and ash particle, respectively. The local radiative entropy generation rate related to absorbance and emission (S'''_{ae}) is defined as follows:

$$S'''_{ae}(\mathbf{r}) = S'''_{ae,CO_2}(\mathbf{r}) + S'''_{ae,H_2O}(\mathbf{r}) + S'''_{ae,soot}(\mathbf{r}) + S'''_{ae,ac}(\mathbf{r}) \quad (13)$$

The scattering process of unburnt char and ash particle is considered in the paper. The local entropy generation (S'''_s) due to this scattering process can be calculated as [8,12]:

$$S'''_s(\mathbf{r}) = \sum_{\text{bands}}\int_\Omega\sum_{i=1}^{N_q}\sum_{j=1}^{N_q}\omega_i\omega_j\sigma_{\eta,\text{ac}}\left(\frac{1}{4\pi}\int_{\Omega'}\frac{I_{\Delta\eta}(\mathbf{r},\mathbf{s}')}{T_\eta(\mathbf{r},\mathbf{s}')}\Phi(\mathbf{s},\mathbf{s}')d\Omega' - \frac{I_{\Delta\eta}(\mathbf{r},\mathbf{s})}{T_\eta(\mathbf{r},\mathbf{s})}\right)d\Omega\Delta\eta \quad (14)$$

In addition, the local entropy generation due to the irreversibility of the absorption, emission, and reflection processes at the wall is given as [8,12]:

$$S''_W(\mathbf{r}_W) = \sum_{\text{bands}}\int_\Omega\sum_{i=1}^{N_q}\sum_{j=1}^{N_q}\omega_i\omega_j\left[\frac{I_{\Delta\eta,ij}(\mathbf{r}_W,\mathbf{s})}{T_W} - L_\eta(\mathbf{r}_W,\mathbf{s})\right](\mathbf{n}_W,\mathbf{s})d\Omega\Delta\eta \quad (15)$$

where $L_\eta(\mathbf{r}_w,\mathbf{s})$ is the spectral radiative entropy intensity, and T_W is the temperature of the wall. The total radiative entropy generation can be defined as the sum of the local terms, as follows:

$$S_G = \int_V S'''_{ae}(\mathbf{r}) + S'''_s(\mathbf{r})dV + \int_A S'''_W(\mathbf{r}_W)dA \quad (16)$$

Table 1
Conditions of six cases.

Case	Oxidizer atmosphere	Coal burnout rate		Volume fraction		Coal diameter D_p
		t_B	k_B	$f_{v,ac}$	$f_{v,soot}$	
1	Air-based, dry gas, and wet gas fuels	0.8	1.0	20 ppm	2 ppm	40μm
2	Air-based fuel	0.9, 0.8, 0.7, 0.6,0.5,	1.0	20 ppm	2 ppm	40μm
3	Air-based fuel	0.8	0.8, 0.85, 0.9, 0.95,1.0	20 ppm	2 ppm	40μm
4	Air-based fuel	0.8	1.0	10, 20, 30, 40, 50 ppm	2 ppm	40μm
5	Air-based fuel	0.8	1.0	20 ppm	1, 2, 3, 4, 5 ppm	40μm
6	Air-based fuel	0.8	1.0	20 ppm	2 ppm	20, 40, 60, 80, 100 μm

Furthermore, based on the calculation of the REGR, the dimensionless entropy generation (M) characterizing the degree of irreversibility of the radiative heat transfer process is expressed as:

$$M = \frac{S_G \cdot T_0}{Q} \tag{17}$$

where S_G is the total radiative entropy generation and T_0 is the ambient temperature, which is set to 300 K. The local dimensionless wall entropy generation, defined as $M''_W(\mathbf{r}_W) = T_0 S''_W(\mathbf{r}_W)/q(\mathbf{r}_W)$, was also calculated to reflect the degree of irreversibility of the radiative heat transfer process at the wall. Furthermore, to analyze the role of the particles in radiative heat transfer, we set the ratio of the volumetric REGR due to particle radiation to the total volumetric radiative entropy generation (χ_p). This is expressed as follows:

$$\chi_p = \frac{S_{vol,p}}{S_{vol}} = \frac{S_{ae,soot} + S_{ae,ac} + S_{s,p}}{S_{ae,soot} + S_{ae,ac} + S_{ae,CO_2} + S_{ae,H_2O} + S_{s,p}} \times 100\% \tag{18}$$

3. Description of the cases

In order to perform a realistic analysis of the radiative entropy generation in a 3-D coal-fired furnace, numerical calculations were performed with the prescribed concentrations and temperature profiles derived from a simplified combustion calculation for a coal-fired furnace [35]. The radiative entropy heat transfer equations for a 3-D real-size (labeled Furnace B with dimensions of $L_x \times L_y \times L_z = 20$ m $\times$ 20 m $\times$ 50 m) virtual coal-fired furnace were solved, and to demonstrate the effect of optical thickness on the REGR, another small furnace with dimensions of 0.2 m $\times$ 0.2 m $\times$ 0.5 m (labeled Furnace A) was also considered. The calculation domain was uniformly divided into 40 $\times$ 40 $\times$ 100 grids. Meanwhile, the thermal radiation was calculated in the spectral range of 20–11,200 cm^{-1}, which covers the entire infrared spectrum. Six cases were set to analyse the influences of the oxidizer atmosphere in the furnaces, the burnout rate, as well as the concentrations of soot ($f_{v,soot}$), unburnt char and ash ($f_{v,ac}$) on radiative entropy generation, respectively. The conditions of these cases are given in Table 1.

4. Results and discussion

4.1. Distributions of local radiative entropy generation

The distributions of S'''_{ae,CO_2}, S'''_{ae,H_2O}, $S'''_{ae,soot}$, and $S'''_{ae,ac}$ in Furnace A, for the air-based atmosphere in Case 1, are shown in Fig. 1. It can be seen from Fig. 1(a) that along the axial centre line of the furnace, the value of S'''_{ae,CO_2} reaches a peak near the location of the highest temperature of the medium. However, the peak values of S'''_{ae,H_2O}, $S'''_{ae,soot}$ and $S'''_{ae,ac}$ are located at the inlet of Furnace A, and gradually decrease downstream of the flame, reaching their minimum values at the exit of the furnace. The values of S'''_{ae,CO_2}, S'''_{ae,H_2O}, $S'''_{ae,soot}$ and $S'''_{ae,ac}$ are higher in the axial direction between the centre line and the walls, and are slightly lower at the centre line. The value of S'''_S is higher near the walls, and shows oscillations in the z-direction, as well as an overall decrease with an increase in height.

The distributions of S'''_{ae,CO_2}, S'''_{ae,H_2O}, $S'''_{ae,soot}$, and $S'''_{ae,ac}$ in Furnace B are shown in Fig. 2. All of the distributions change significantly as the size of the furnace increases, and their values are higher near the walls and lower inside the furnace. The reason for this is that with an increase in the dimensions of the furnace, the radiative heat transfer process in the furnace gradually develops towards thermal diffusion, and the effect of the local temperature gradient on the thermal radiation gradually increases [3]. In addition, the medium near the wall of the furnace has a high temperature gradient, resulting in an intense radiative heat transfer process and high irreversibility in this region. When evaluating the local radiative entropy generation distributions of both furnaces, the values of REGR of Furnace B are quite high compared to Furnace A,

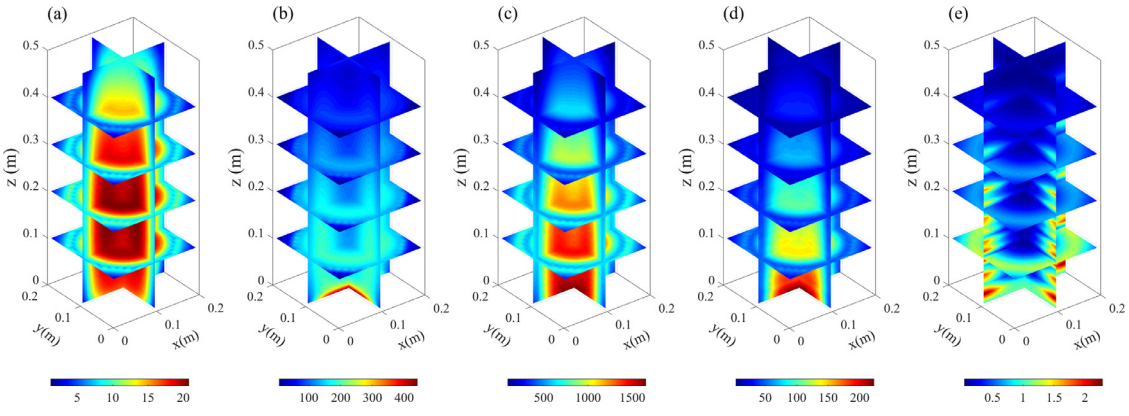


Fig. 1. Three-dimensional distributions of (a) S'''_{ae,CO_2}, (b) S'''_{ae,H_2O}, (c) $S'''_{ae,soot}$, (d) $S'''_{ae,ac}$, and (e) S'''_s for Furnace A in Case 1.

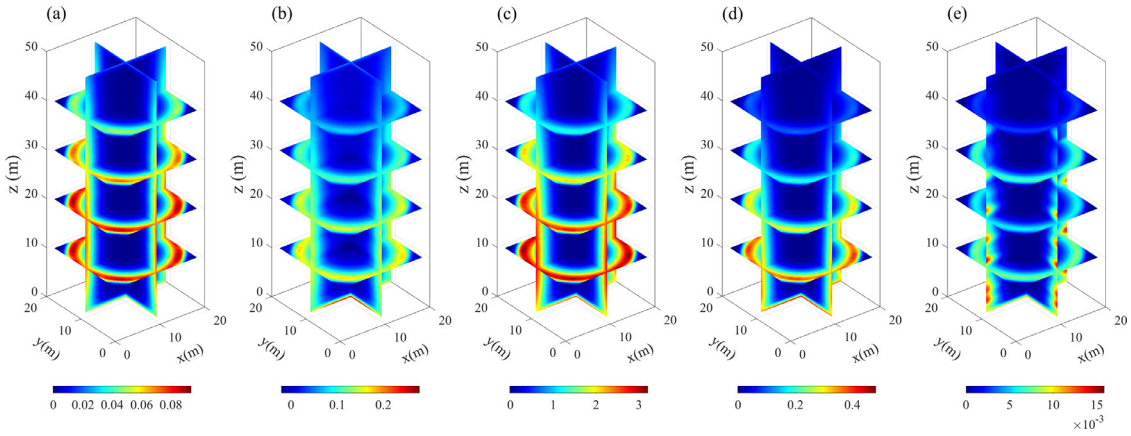


Fig. 2. Three-dimensional distributions of (a) S'''_{ae,CO_2}, (b) S'''_{ae,H_2O}, (c) $S'''_{ae,soot}$, (d) $S'''_{ae,ac}$, and (e) S'''_s for Furnace B in Case 1.

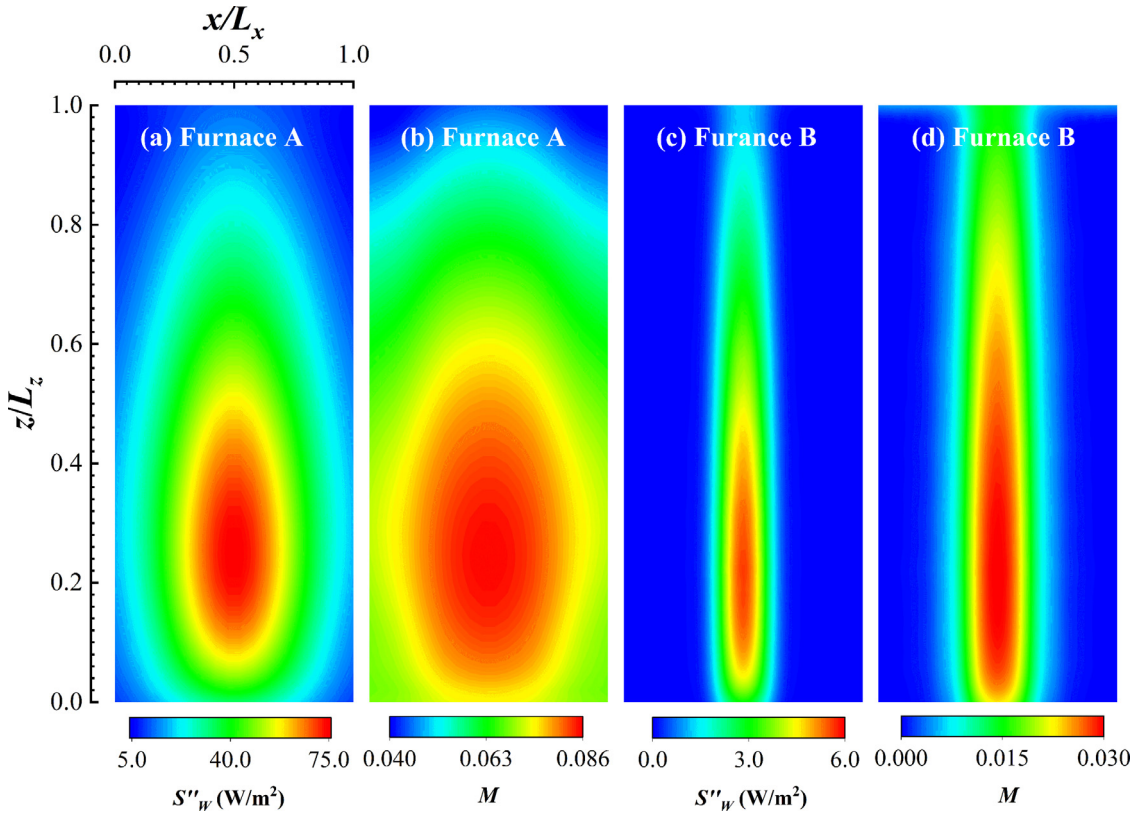


Fig. 3. Distributions of S''_W and M''_W in Furnaces A and B in Case 1.

because the dimensions of Furnace B are one hundred times larger than that of Furnace A.

The behaviour of S''_W for Furnaces A and B is shown in Fig. 3(a) and (c). It can be seen that in the z-direction, S''_W increases with a rise in the temperature of the medium, and then decreases towards the outlet of the furnace. The values of S''_W for Furnaces A and B reach a maximum at the centre line, which is upstream of the highest temperature. In the x-direction, the S''_W distributions on the wall undergo considerable changes as the dimensions of the furnace change. In Furnace B, S''_W increases significantly when the x coordinate is in the range 8–12 m, while it is lower in the other regions. However, in Furnace A, S''_W is low only near the exit of the furnace, and the radiative heat transfer in the other regions produces a relatively high S''_W.

The distributions of M''_W for Furnaces A and B in Case 1 are given in Fig. 3(b) and (d). In general, M''_W is higher for Furnace A than for Furnace B. The value of M''_W for Furnace A reaches 0.086. It is noteworthy that the degree of irreversibility of the radiative heat transfer process is higher at the underside of the wall, where the temperature of the medium is high, and is lower in the region near the exit and at the edge of the furnace.

4.2. Effect of the oxidizer atmosphere

The numerical calculations of REGR were carried out under three types of combustion conditions, namely, a typical air-based coal-fired furnace and two oxy-fuel atmospheres with dry and wet gas. The values of S_{ae,CO_2}, S_{ae,H_2O}, $S_{ae,soot}$, $S_{ae,ac}$, and S_G under different conditions for Furnaces A and B in Case 1 are shown in Fig. 4(a) and (b). There is no significant different between the values of $S_{ae,soot}$ and S_W in Furnace A. However, the value of S_W is significantly lower than $S_{ae,soot}$ in Furnace B. Due to the increase

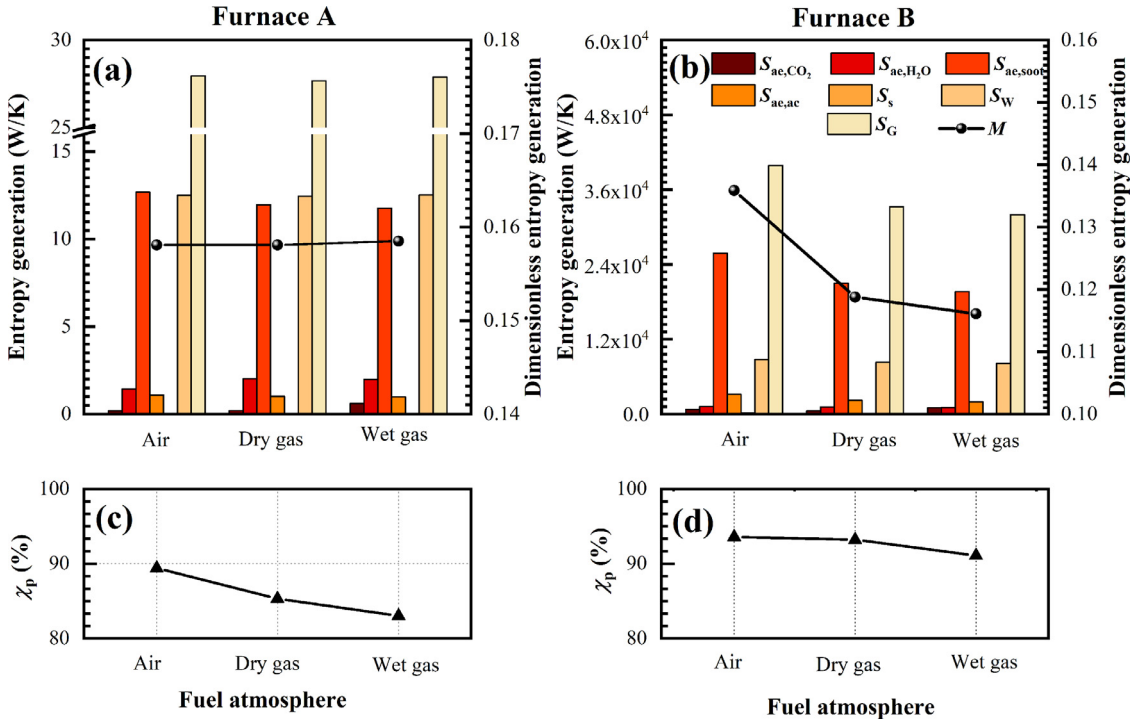


Fig. 4. Values of S_{ae,CO_2}, S_{ae,H_2O}, $S_{ae,soot}$, $S_{ae,ac}$, S_G, M, and χ_p for Case 1.

in gas concentration, the values of S_{ae,CO_2} and S_{ae,H_2O} also increase and $S_{ae,soot}$ decreases slightly when the oxidizer atmosphere changes from air to dry or wet gas. M decreases as the oxidizer atmosphere changes from air to dry or wet gas, and reaches a minimum value in the wet gas atmosphere for Furnace B.

The ratios χ_p under different oxidizer atmospheres for Furnaces A and B are given in Fig. 4(c) and (d). It can be seen that χ_p exceeds 80% of the total volumetric entropy generation, and reaches more than 90% in Furnace B for all fuel atmospheres. This indicates that particles have a much greater impact on the irreversibility of radiative heat transfer than gases, and hence should not be ignored in the thermodynamics of the combustion process.

4.3. Effects of the burnout rate of pulverized coal

The S values for H_2O, CO_2, soot, unburnt char and ash particle and the M values under the various conditions in Case 2 are shown in Fig. 5. It can be seen that the value of S_G in the furnaces increases significantly with an increase in the burnout rate. For example, in Furnace A, it increases by 31.6% and 33.3% as the burnout rate factor (t_B) increases from 0.1 to 0.5. The values of $S_{ae,soot}$ increase due to the radiative process at the wall. M increases with an increase in the burnout rate factor, indicating that the degree of irreversibility of the radiative heat transfer process gradually increases as the burnout rate increases.

The changes in the values of χ_p for Furnaces A and B with the burnout rate factor (t_B) are given in Fig. 5(c) and (d), respectively. It can be seen that the values of χ_p are approximately 89% in Furnace A and 94% in Furnace B. The results do not change significantly for different values of t_B.

The changes in the S values of the parameters and the M values in Case 3 under various conditions with the burnout degree factor (k_B) are shown in Fig. 6. The values of S_G and $S_{ae,soot}$ gradually increase further in Furnaces A and B. In addition, M also increases with an increase in the burnout degree factor in Furnace B, illustrating the degree of irreversibility of the radiative heat transfer process. The value of M decreases with an increase in the burnout degree factor in Furnace A.

The $\chi_p$ratios for Furnaces A and B are given in Fig. 6(c) and (d), respectively. The values of χ_p are approximately 84% and 92% of the total volumetric entropy generation in Furnaces A and B, respectively, and the results do not change significantly for different degrees of coal burnout.

4.4. Effect of the volume fraction of particles

The values of S for H_2O, CO_2, soot, unburnt char and ash particle, and the values of M under the various conditions in Case 4 are shown in Fig. 7. It can be seen that the values of S_G for both furnaces increase gradually with an increase in the volume fraction of unburnt char and ash particle. In Furnace A, the effect of the volume fraction of unburnt char and ash particle on S_G and M is low, and S_G increases by only 5.6% in Furnace A, whereas it increases by 41% in Furnace B. The value of M increases only slightly in Furnace A with increasing volume fraction, while in Furnace B it increases significantly.

The ratios χ_p for different volume fractions of unburnt char and ash particle in Furnaces A and B are given in Fig. 7(c) and (d), respectively. It can be seen that a change in the volume fraction of unburnt char and ash particle does not have a significant effect on χ_p. When the volume fraction of unburnt char and ash particle is increased from 10 to 50 ppm, the proportion of the REGR due to particle radiation increases from 89.0% to 90.3% in Furnace A, but decreases from 94.1% to 92.0% in Furnace B.

The effects of the concentrations of soot ($f_{v,soot}$) and char particles ($f_{v,ac}$) on S and M under various conditions in Case 5 are shown in Fig. 8. It can be seen that the volume fraction of soot has an important effect on the radiative heat transfer process in Furnace A, especially when $f_{v,soot}$ is low. When the soot volume fraction is increased from 1 to 5 ppm, the REGR increases by 45.3% in Furnace A. Although $f_{v,soot}$ is small in Furnace B, high values of M are obtained, and as $f_{v,soot}$ is increased, M decreases by 70% in

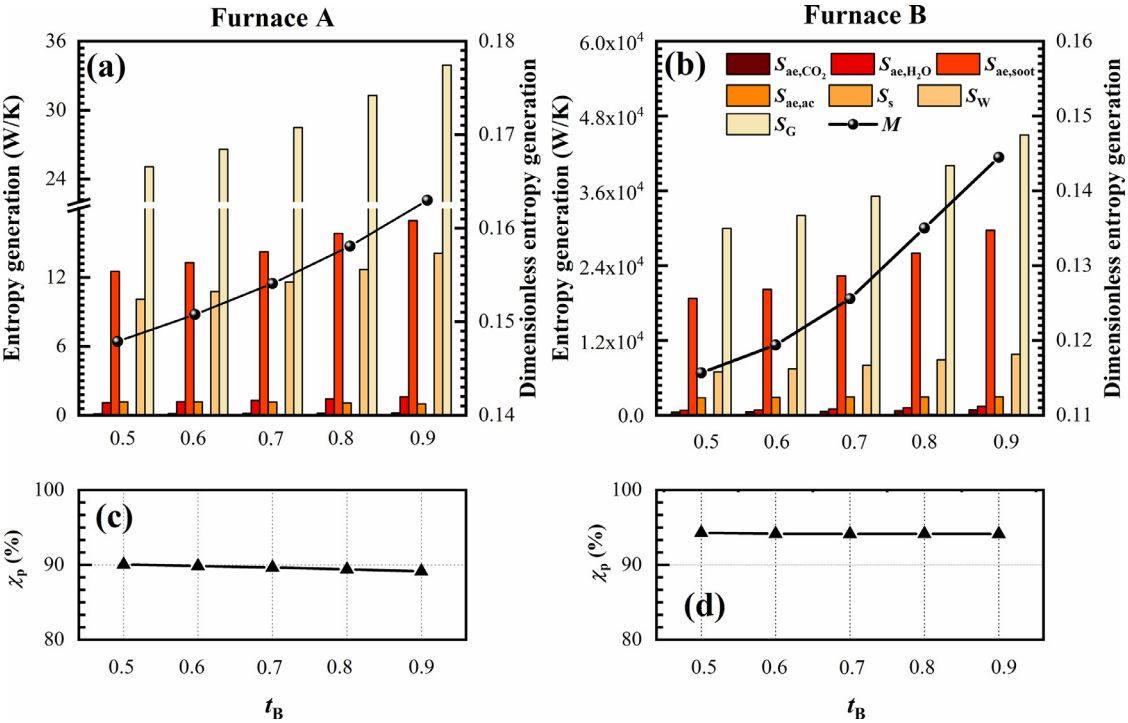


Fig. 5. Values of S_{ae,CO_2}, S_{ae,H_2O}, $S_{ae,soot}$, $S_{ae,ac}$, S_G, M, and χ_p for Case 2.

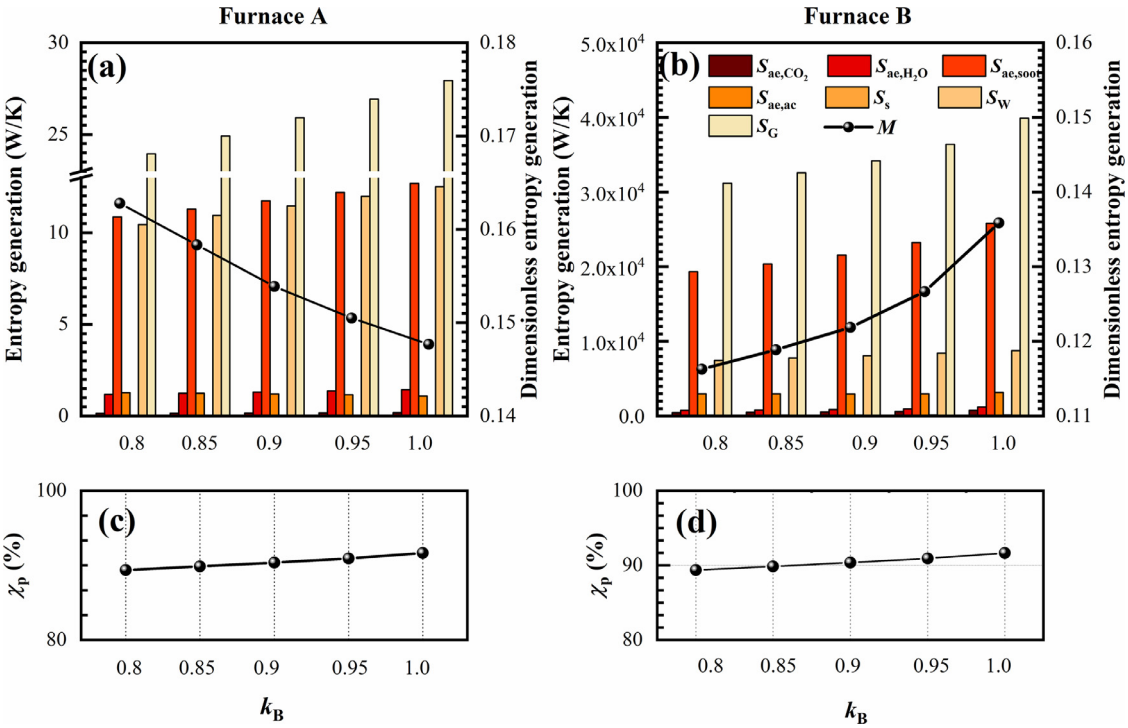


Fig. 6. Values of S_{ae,CO_2}, S_{ae,H_2O}, $S_{ae,soot}$, $S_{ae,ac}$, S_G, M, and χ_p for Case 3.

Furnace B. The values of $S_{ae,soot}$ and S_G decrease gradually with an increase in $f_{v,\mathrm{soot}}$ in Furnace B, whereas they increase with $f_{v,\mathrm{soot}}$ in Furnace A. Finally, M increases in Furnace A but decreases in Furnace B as $f_{v,\mathrm{soot}}$ is increased from 1.0 to 6.0 ppm. Ref [9], using the results of a highly accurate numerical method, it was concluded that the level of interaction between matter and radiation and strong changes in material properties affect the distributions of S_G. Although the material properties are the same in both furnaces in our study, since the optical thickness of Furnace B is larger than that of Furnace A, as mentioned in [9], the values of S_G decrease in Furnace B due to the smaller matter-radiation interaction based on its large size in contrast to Furnace A. The ratios χ_p under different soot volume fractions in Furnaces A and B are shown in Fig. 8(c) and (d), respectively. The REGR due to particle radiation increases with the soot volume fraction. When the soot volume fraction is only 1.0 ppm, the proportion of the REGR due

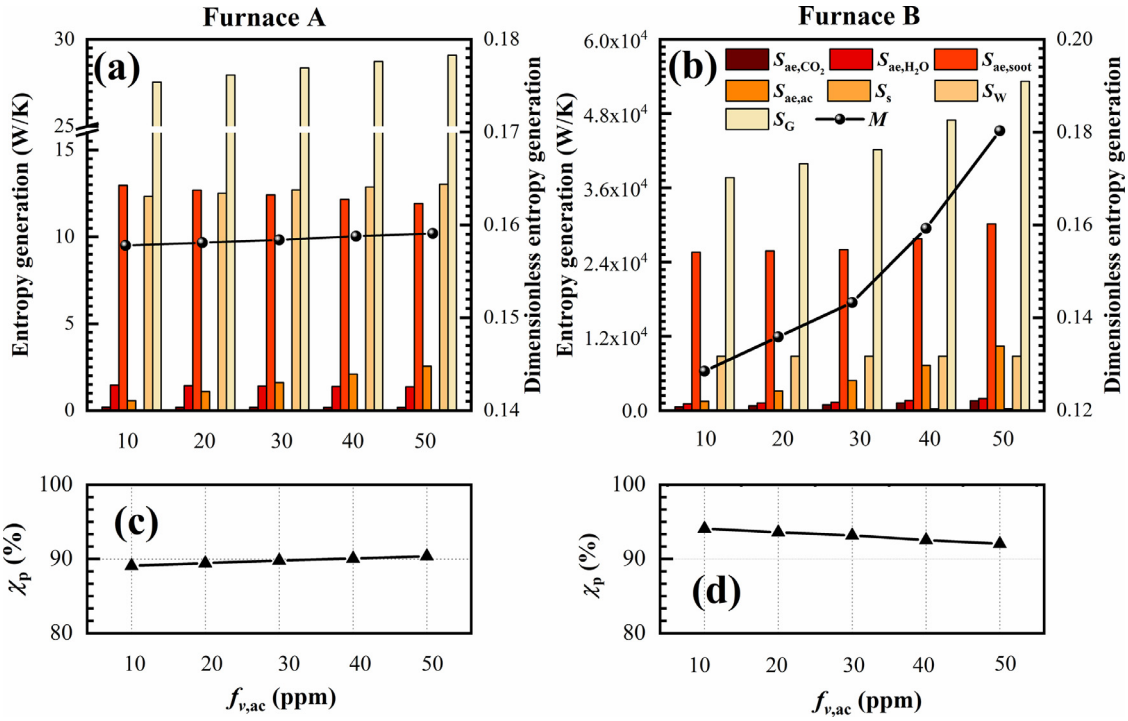


Fig. 7. Values of S_{ae,CO_2}, S_{ae,H_2O}, $S_{ae,soot}$, $S_{ae,ac}$, S_G, M and $\chi_p$for Case 4.

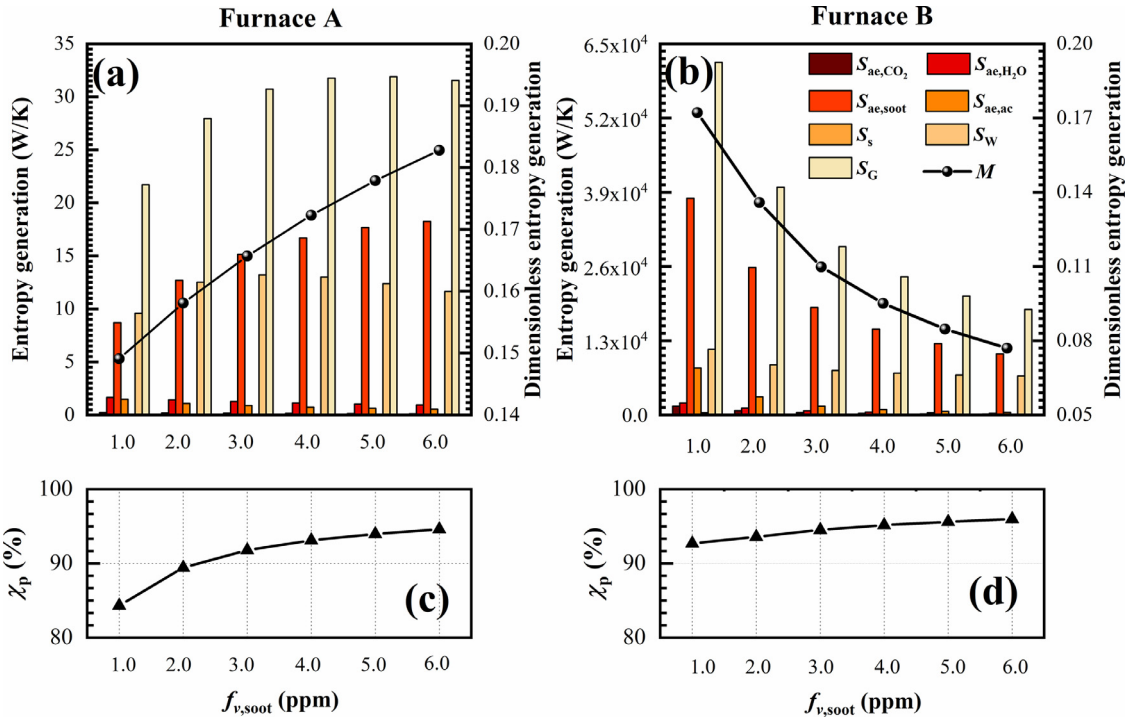


Fig. 8. Changes in S_{ae,CO_2}, S_{ae,H_2O}, $S_{ae,soot}$, $S_{ae,ac}$, S_G, M, and χ_p in Case 5.

to particles in Furnaces A and B is 84.3% and 89.1%, respectively, whereas when the soot volume fraction is 6.0 ppm, this reaches 94.6% in both furnaces. This further illustrates the important role of the particles and the irreversibility of the radiation process.

4.5. Effect of the particle size distribution

The values of S_{ae,CO_2}, S_{ae,H_2O}, $S_{ae,soot}$ and $S_{ae,ac}$, S_G and the M in Case 6 under various conditions are shown in Fig. 9. As can be seen in Fig. 9, as the initial diameter of pulverized coal particles increases from 20 to 100 μm, S_G decreases by 9.7% in Furnace A. In Furnace B, on the other hand, it decreases as the diameter of the pulverized coal particles increases, reaches its lowest value when the initial diameter of the particles is 60 μm, and then increase slightly as the particle diameter increases further. In Furnace A, the values of S_{ae,CO_2}, S_{ae,H_2O} and $S_{ae,soot}$ are almost identical to an increase in the initial diameter of the particle. The values of $S_{ae,ac}$ for both furnaces decrease with the particle diameter. Moreover,

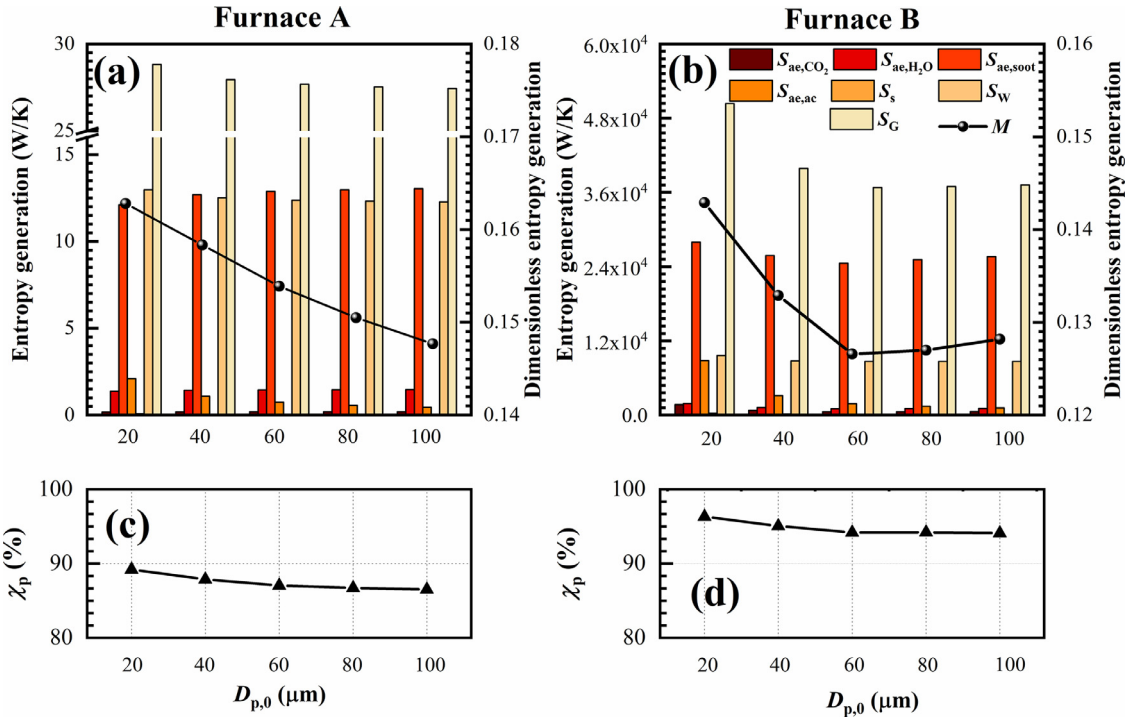


Fig. 9. The values of S_{ae,CO_2}, S_{ae,H_2O}, $S_{ae,soot}$, $S_{ae,ac}$, S_G and M, χ_p in Case 6.

the M also showed a trend of first decreasing and then increasing with increasing particle diameter in Furnace B. When the initial particle diameter of pulverized coal was 60 μm, M reached its lowest value. The $\chi_p$ratios in Furnaces A and B change with the particle diameter as shown in Fig. 9(c) and (d), respectively. When the initial diameter of the particles increases from 20 to 100 μm, χ_p in Furnace A decreases slightly from 89.2% to 86.5%. In Furnace B, on the other hand, it decreases slightly from 96.3% to 94.1%.

4. Conclusion

The radiative entropy generation in a three-dimensional coal-fired furnace was investigated. The local radiative entropy generation was given and the contributions of different components of the mixed medium including CO_2, H_2O, soot, unburnt char and ash to the total radiative entropy generation were calculated. The effects of the oxidizer atmosphere, burnout rate of pulverized coal particles, and the volume fraction of soot, unburnt char and ash on the radiative entropy generation were analysed. Some key conclusions can be provided as follows:

1. For furnaces with different dimensions, there are obvious differences in the distributions of the local entropy S'''_{ae,CO_2}, S'''_{ae,H_2O}, $S'''_{ae,soot}$, $S'''_{ae,ac}$, and S'''_s. The maximum values of the local entropy generations of Furnace A are 20.74, 349.45, 1632.25, 214.33 and the total S_G value is 2213.87 W/m^{3}K, respectively. The maximum values of the local entropy generations of Furnace B are 0.094, 0.289, 3.211, 0.483 and the total S_G value is 3.891 W/m^{3}K, respectively. These values are high inside the furnace when the furnace is small. However, when the furnace is large, the values near the furnace wall are high due to the large temperature gradient.
2. The ratio χ_p is more than 80% of the volumetric radiation entropy generation for all cases considered in this paper and the value increases significantly when the concentration of soot increases. The particles have a much greater impact on the radiative entropy generation than gases.
3. In a real-size furnace ($L_x \times L_y \times L_z$ = 20 m × 20 m × 50 m), S_G decreases when wet gas is used as the circulating gas, and it increases with the burnout rate. The concentration of particles also has an important effect on REGR, which decreases by 41% when the concentration of unburnt char and ash increases from 10 ppm to 50 ppm and decreases by 70% when concentration of soot increases from 1 ppm to 5 ppm. This is because the interaction between particles and radiation in the furnace is lessened.
4. For all furnaces, S_G increases linearly with the burnout rate factor (t_B=0.5–0.9), burnout degree factor (k_B=0.8–1) and char volume fraction (10–50 ppm). .

Authorship contribution statement

Zhongnong Zhang (First Author): Conceptualization, Methodology, Software, Formal analysis, Investigation, Writing - original draft, review & editing.

Nimeti Doner (Corresponding Author): Methodology, Writing - original draft, Writing - review & editing.

Chun Lou (Corresponding Author): Conceptualization, Funding acquisition, Resources, Supervision, Validation, Writing - review & editing.

Chong Zhang: Conceptualization, Investigation.

Declaration of Competing Interest

The authors declare that they have no known competing financial interests or personal relationships that could have appeared to influence the work reported in this paper.

Data availability

No data was used for the research described in the article.

Acknowledgments

This work was supported by the National Natural Science Foundation of China (No. 51827808). The computing work in this paper was supported by the HPC public service platform provided by Network and Computing Center of HUST.

Appendix A. Distributions of participating species

The properties of the participating species (the temperature of the medium, and the distribution functions of the gas, fly ash and char) in a furnace were calculated based on the formulations given in Ref. [35], The distributions of the gas concentration and the temperature of the medium were derived according to a simplified combustion calculation in a three-dimensional coal-fired furnace [34,35]. The parameters needed to calculate the distributions of the gas concentration are given in Table A.1. These thermodynamic parameters are considered to have completely symmetrical distributions, and are given as:

$$\Theta(\mathbf{r}) = f_r(\mathbf{r})\Theta_W + (1 - f_r(\mathbf{r}))\Theta_C \tag{A.1}$$

where Θ is the distribution including the gas concentration and the temperature of the medium. The subscripts W and C indicate the positions along the wall and the centerline, respectively. The radial factor f_r is defined as:

$$f_r(\mathbf{r}) = \left(\min\left(\frac{2r}{L_x}, 1\right)\right)^3 \tag{A.2}$$

where $r = [(x - L_x/2)^2 + (y - L_y/2)^2]^{0.5}$ is the distance to the centerline, and L_x and L_y are the length and width of the three-dimensional enclosure, respectively.

Based on the symmetrical distributions in Eq. (A.1), the distributions of CO_2 and H_2O along the wall and centerline are given as:

$$\begin{aligned}\Theta_{W,mf} &= B_{fly}\Theta_{fly,mf} + B_{\text{char}}\Theta_{\text{char},mf} + \Theta_{in,mf}\\ \Theta_{C,mf} &= B_{\text{char}}\left(\Theta_{\text{char},mf} + \Theta_{fly,mf}\right) + \Theta_{in,mf}\end{aligned} \tag{A.3}$$

where $\Theta_{W,mf}$ and $\Theta_{\text{char},mf}$ are the distributions of unburnt char and ash generated by combustion, and $\Theta_{in,mf}$ is the distribution entering the enclosure. B_{fly} and B_{char} are the burnout ratios of unburnt char and ash, which are defined as:

$$B_{fly} = (z/L_z)^{0.2},\ B_{\text{char}} = k_B(z/L_z)^{1-t_B}. \tag{A.4}$$

Here, L_z is the height of the enclosure, and two parameters (the burnout rate factor t_B and the burnout degree factor k_B) were set to adjust the burnout rate and burnout degree of the pulverized coal, respectively. Herein, the burnout rate (t_B) is approximately the change in particle size during combustion ($t_B \sim [-d(D_p^2)/dt]$) [36]. The burnout degree factor (k_B) is the change in coal mass during combustion, and it is also related with the efficiency of the combustion: $k_B = 1 - D_{p,out}/D_{p,initial}$ [37]. The temperature of the medium along the centerline is given as:

$$T_C = (1 - f_a)\left[B_{fly}\frac{T_{ad}}{2} + B_{\text{char}}\frac{T_{ad}}{2} + \left(2 - B_{fly} - B_{\text{char}}\right)T_{in}\right] + f_a T_{exit} \tag{A.5}$$

where $f_a = z/L_z$ is the axial factor. T_{ad}, T_{in}, and T_{exit} represent the adiabatic temperature, inlet temperature and exit temperature of the medium, and were set to 2663, 600, and 1523 K, respectively. Meanwhile, the front, rear, left, and right walls of the enclosure

Table A.1
Parameters related to gas concentration [35].

	Air-based fuel	Dry gas fuel	Wet gas fuel
$X_{in,CO2}$	0	0.7805	0.5057
$X_{fly,CO2}$	0.0636	0.0404	0.4110
$X_{char,CO2}$	0.0909	0.1128	0.1145
$X_{in,H2O}$	0	0	0.2436
$X_{fly,H2O}$	0.0744	0.1020	0.0635
$X_{char,H2O}$	0	0	0

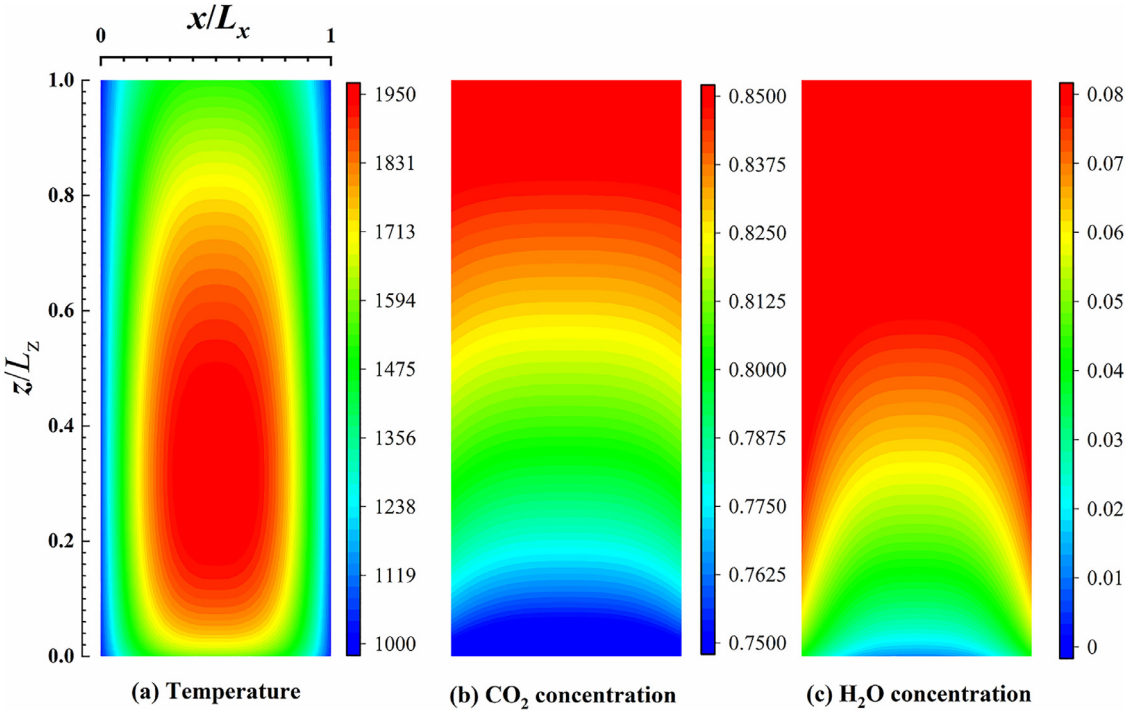


Fig. A.1. Distributions of (a) the temperature of the medium; (b) CO_2; (c) H_2O [35].

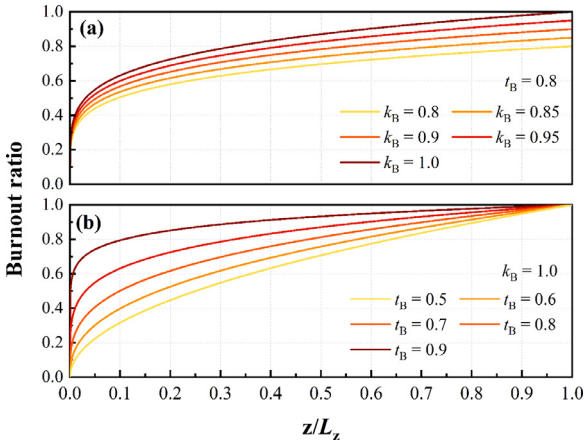


Fig. A.2. Distributions of the pulverized coal burnout rate with furnace height for different values of t_B and k_B [29].

were considered to be black and their temperature was set to 973 K. The inlet and outlet of the enclosure were also considered to be black walls; the temperature of the inlet set was set to 600 K, and that of the outlet to 1223 K.(Fig. A1)

The distributions of the pulverized coal burnout rate with furnace height are shown in Fig. A.2 for different parameter values. It can be seen that the burnout rate and burnout degree of the pulverized coal gradually increase as the burnout rate factor decreases and the burnout degree factor increases. To illustrate the importance of the effects of the burnout ratio and burnout degree of the particles, the changes in unburned char with dimensionless length are presented in Fig. A.2.

Appendix B. Validation of the radiation model

To verify our numerical results, three combustion cases were simulated. In these cases, fuels under air-based, dry-gas, and wet-gas atmospheres were considered, and the parameters of these fuels are given in Table A.1. The burnout rate factor t_B and burnout degree factor k_B were set to 0.2 and 1.0, respectively. These cases were calculated numerically in previous work using the narrow-band correlated-k model [35]. The values of the net wall heat flux in the y-direction at the centerline obtained in this study and in previous work are shown in Fig. B.1. It can be seen that the numerical results obtained in this paper show good agreement with the results reported in reference [35].

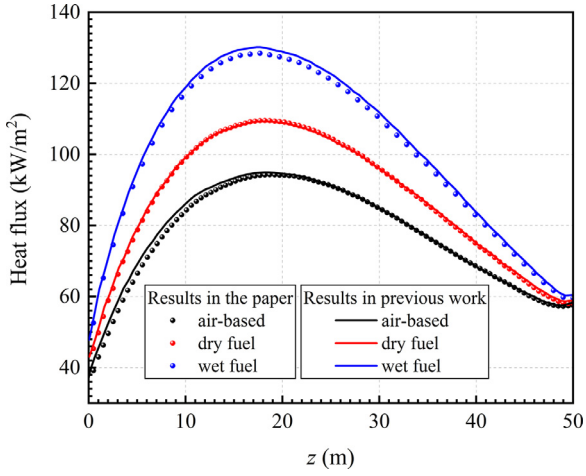


Fig. B.1. Net wall heat flux in the y-radial direction at the centerline.

References

[1] M.J. Moran, H.N. Shapiro, D.D. Boettner, M.B. Bailey, Fundamentals of Engineering Thermodynamics, Wiley, 2018.
[2] A. Sciacovelli, V. Verda, E. Sciubba, Entropy generation analysis as a design tool - a review, Renew. Sust. Energy Rev. 43 (2015) 1167–1181.
[3] M. Modest, Radiative Heat Transfer, 3rd edition, Academic Press, San Diego, 2013.
[4] S.K. Som, A. Datta, Thermodynamic irreversibilities and exergy balance in combustion processes, Prog. Energy Combust. Sci. 34 (2008) 351–376.
[5] A. Agudelo, C. Corte, Thermal radiation and the second law, Energy 35 (2010) 679–691.
[6] M. Plank, The Theory of Heat Radiation, Dover, 1959.
[7] S. Wright, M. Rosen, D. Scott, J. Haddow, The exergy flux of radiative heat transfer for the special case of blackbody radiation, Exergy Int. J. 2 (2002) 24–33.
[8] Z.M. Zhang, S. Basu, Entropy flow and generation in radiative transfer between surfaces, Int. J. Heat Mass Transf. 50 (2007) 702–712.
[9] M. Caldas, V. Semião, Entropy generation through radiative transfer in participating media: analysis and numerical computation, J. Quant. Spectrosc. Radiat. Transf. 96 (3–4) (2005) 427–437.
[10] M. Caldas, V. Semião, The effect of turbulence-radiation interaction on radiative entropy generation and heat transfer, J. Quant. Spectrosc. Radiat. Transf. 104 (1) (2007) 12–23.
[11] L.H. Liu, S.X. Chu, On the entropy generation formula of radiation heat transfer processes, J. Heat Transf. 128 (5) (2006) 504–506.
[12] L.H. Liu, S.X. Chu, Verification of numerical simulation method for entropy generation of radiation heat transfer in semitransparent medium, J. Quant. Spectrosc. Radiat. Transf. 103 (1) (2007) 43–56.
[13] C. Lou, Z.N. Zhang, Experimental and numerical analysis of radiative entropy generation in industrial and boiler furnace, J. Quant. Spectrosc. Radiat. Transf. 232 (2019) 27–34.
[14] Z.N. Zhang, Z.C. Li, C. Lou, Numerical analysis of radiative entropy generation in a parallel plate system with non-uniform temperature distribution participation medium, J. Quant. Spectrosc. Radiat. Transf. 225 (2019) 319–326.
[15] A. Bahrami, A. Safavinejad, H. Amiri, Analysis of spectral radiative entropy generation in a non-gray planar participating medium at radiative equilibrium with two different boundary conditions, Int. J. Therm. Sci. 146 (2019) 1060–1073.
[16] Z.N. Zhang, C. Lou, Z. Li, Y. Long, Evaluation of radiative entropy generation in a high temperature system including H_2O, CO_2 and soot with non-gray wall, J. Quant. Spectrosc. Radiat. Transf. 253 (2020) 107175.
[17] R. Johansson, B. Leckner, K. Andersson, F. Johnsson, Influence of particle and gas radiation in oxy-fuel combustion, Int. J. Heat Mass Tran. 65 (2013) 143–152.
[18] V. Kez, J. Consalvi, F. Liu, T. Gronarz, J. Ströhle, R. Kneer, Bernd Epple, Investigation of gas and particle radiation modelling in wet oxy-coal combustion atmospheres, Int. J. Heat Mass Tran. 133 (2019) 1026–1040.
[19] M.S. Yasar, G. Ozen, N. Selçuk, G. Kulah, Assesment of improved banded model for spectral thermal radiation in presence of non-gray particles in fluidized bed combustors, Appl. Therm. Eng. 176 (2020) 115322.
[20] J. Taine, A line by line calculation of low-resolution radiative properties of CO_2-CO-transparent non-isothermal gas mixtures up to 3000 K, J. Quant. Spectrosc. Radiat. Transfer 30 (1983) 371–379.
[21] T.F. Smith, Z.F. Shen, J.N. Friedman, Evaluation of coefficients for the weighted sum of gray gases model, J. Heat Transf. 104 (4) (1982) 602–608.
[22] F. Liu, G.J. S.mallwood, O.L. Gülder, Application of the statistical narrow-band correlated-k method to low-resolution spectral intensity and radiative heat transfer calculations-effects of the quadrature scheme, Int. J. Heat Mass Transf. 43 (2000) 3119–3135.
[23] R.P. Gupta, T.F. Wall, The optical properties of fly ash in coal fired furnaces, Combust. Flame 61 (2) (1985) 145–151.
[24] D.G. Goodwin, M. Mitchner, Fly ash radiative properties and effects on radiative heat transfer in coal-fired systems, Int. J. Heat Mass Trans. 32 (4) (1989) 627–638.
[25] P.J. Foster, C.R. Howarth, Optical constants of carbons and coals in the infrared, Carbon N Y 6 (1968) 719–724.
[26] D. Baillis, J.F. Sacadura, Thermal radiation properties of dispersed media: theoretical prediction and experimental characterization, J. Quant. Spectrosc. Radiat. Transf. 67 (2000) 327–363.
[27] J. Guo, F. Hu, W. Luo, P. Li, Z. Liu, A full spectrum k-distribution based non-gray radiative property model for unburnt char, P. Combust. Inst. 37 (2019) 3081–3089.
[28] N. Doner, N. Selçuk, An application of spectral line-based weighted sum grey gases (SLW) model with geometric optics approximation for radiative heat transfer in 3-D participating media, Appl Therm Eng 50 (2013) 89–93.
[29] C.F. Bohren, D.R. Huffman, Absorption and Scattering of Light by Small Particles, Wiley, Weinheim, 1998.
[30] E. Sutcu, N. Doner, F. Liu, U. Ercetin, F. Sen, J. Yon, J. Morán, A. Fuentes, Morphological and radiative characteristics of soot aggregates: experimental and numerical research, Sci. Rep. 10 (2020) 411.

[31] S. Yagi, H. Iino, Radiation from soot particles in luminous flames, in: Symposium (International) on Combustion, 8, 1961, pp. 288–293.
[32] G.C. Fraga, L. Zannoni, F.R. Centeno, F.H.R. França, Evaluation of different gray gas formulations against line-by-line calculations in two- and three-dimensional configurations for participating media composed by CO_2, H_2O and soot, Fire Safety J. 108 (2019) 102843.
[33] D. Makhanlall, Thermodynamic second-law analysis of radiative heat transfer in two-phase (particulate) media, J. Thermophys. Heat Transf. 27 (2) (2013) 360–363.
[34] J. Strohle, B. Epple, M. Orth, Spectral modelling of radiative heat transfer in oxy-coal combustion, 1st oxyfuel combustion conference, cottbus, Germany, 2009.
[35] V. Kez, J.L. Consalvi, F. Liu, J. Strohle, B. Epple, Assessment of several gas radiation models for radiative heat transfer calculations in a three-dimensional oxy-fuel furnace under coal-fired conditions, Int. J. Therm. Sci. 120 (2017) 289–302.
[36] T.X. Li, D.L. Zhu, N.K. Akafuah, K. Saito, C.K. Law, Synthesis, droplet combustion, and sooting characteristics of biodiesel produced from waste vegetable oils, P. Combust. Inst. 33 (2011) 2039–2046.
[37] M. Zhao, L. Liu, A. Fan, Comparison of combustion efficiency of micro hydrogen jet flames confined in cylindrical tubes of different diameters, Chem. Eng. Process. 153 (2020) 108000.